

# Lithium metal protection through in-situ formed solid electrolyte interphase in lithium-sulfur batteries: The role of polysulfides on lithium anode



Chong Yan <sup>a, b, 1</sup>, Xin-Bing Cheng <sup>b, 1</sup>, Chen-Zi Zhao <sup>b</sup>, Jia-Qi Huang <sup>b, \*</sup>, Shu-Ting Yang <sup>a, \*\*</sup>, Qiang Zhang <sup>b, \*\*\*</sup>

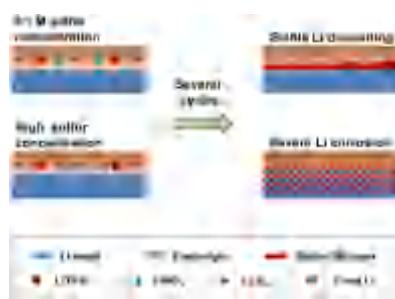
<sup>a</sup> National & Local Joint Engineering Laboratory for Motive Power and Key Materials, College of Chemistry and Chemical Engineering, Henan Normal University, Xinxiang 453007, PR China

<sup>b</sup> Beijing Key Laboratory of Green Chemical Reaction Engineering and Technology, Department of Chemical Engineering, Tsinghua University, Beijing 100084, PR China

## h i g h l i g h t s

- The failure mechanism of Li metal etching at a high sulfur loading in a Li-S cell.
- Excellent electrolyte additives for Li metal anode.
- New understanding towards electrolyte additive design used in Li-S batteries.

## g r a p h i c a l a b s t r a c t



## a r t i c l e i n f o

Article history:  
Received 24 May 2016  
Received in revised form  
13 July 2016  
Accepted 16 July 2016

Keywords:  
Li-S battery  
Polysulfides  
LiNO<sub>3</sub>  
Li metal anode  
Solid electrolyte interphase

## a b s t r a c t

The dissolution and diffusion of Li polysulfide (LiPS) intermediates are regarded as one of the most serious problems for capacity decay and cell failure of lithium-sulfur (Li-S) batteries. Herein we proposed a failure mechanism of Li metal anode in Li-S cells based on the mechanistic investigation into the complex interactions between LiPSs and Li metal. The LiPSs participate the formation of inorganic layers in the solid electrolyte interphase (SEI) in a LiPS-LiNO<sub>3</sub> containing ether-based electrolyte. Li metal anode is well protected by the stable inorganic layer in-situ formed in an electrolyte containing 0.020 M Li<sub>2</sub>S<sub>5</sub> (0.10 M sulfur) and 5.0 wt % LiNO<sub>3</sub>. The metal anode with LiF-Li<sub>2</sub>S<sub>x</sub> riched SEI rendered a stable Coulombic efficiency of 95% after 233 cycles for Li-Cu half cells. A dendrite-free morphology of Li metal anode is observed under the harsh condition. When the LiPS is with a very high concentration of higher than 0.50 M sulfur in the organic electrolyte, the in-situ formed SEI cannot well maintain and the Li metal is gradually etched. Therefore, the polysulfide dissolution and diffusion should be delicately regulated to render a practical Li-S cell when the areal sulfur loading is high.

© 2016 Elsevier B.V. All rights reserved.

\* Corresponding author.

\*\* Corresponding author.

\*\*\* Corresponding author.

E-mail addresses: [jquang@tsinghua.edu.cn](mailto:jquang@tsinghua.edu.cn) (J.-Q. Huang), [shutingyang@foxmail.com](mailto:shutingyang@foxmail.com) (S.-T. Yang), [zhang-qiang@mails.tsinghua.edu.cn](mailto:zhang-qiang@mails.tsinghua.edu.cn) (Q. Zhang).

<sup>1</sup> These authors contributed equally to this work.

## 1. Introduction

The steadily increasing attention toward ultralight portable electronics and electric vehicles stimulates an exponential growth of research interest on advanced rechargeable batteries with high energy/power density, superior safety performance, and long life-span. Unfortunately, the existing lithium-ion batteries, which have dominated the consumer device market, remain insufficient for the strong demand of advanced power sources [1]. Therefore, development of energy-storage systems with high energy density is urgently needed. Among various promising battery candidates, lithium-sulfur (Li-S) batteries with a high theoretical energy density of  $2600 \text{ Wh kg}^{-1}$  are regarded as an attractive alternative [2]. The Li-S batteries also have the outstanding advantages of high natural abundance, low cost, and nontoxicity of sulfur for bulk applications [3–6].

Despite the considerable superiority of Li-S battery, there are several scientific obstacles hindering their practical applications [7–9]: (1) The intrinsically insulate nature of sulfur and the final discharging product ( $\text{Li}_2\text{S}$ ) induces the low utilization of active materials in electrochemical reactions; (2) The shuttle effect and parasitic reaction of Li polysulfide (LiPS) intermediates between anode and cathode leads to the severe capacity decay and poor lifespan of a full Li-S cell; (3) The formation of Li dendrites causes low energy efficiency and hazardous safety problems. By introducing high conductive nanocarbon and polar scaffolds as the cathode matrix, the conductivity of cathode is significantly improved, which makes the sulfur easy to participate the conversion reactions with  $\text{Li}^+$ . The strategies of physical confinement [10–14] and surface chemical adsorption of LiPSs in the cathode [15–19], interlayers [20–22], electrolyte additives [23,24], LiPS redox mediator [25], polyelectrolyte [26], and ion-selective separator [27,28] have been proposed to regulate the dissolution and diffusion of LiPSs. To inhibit dendrite growth on Li metal anode in a Li-S full cell, several strategies, such as electrolyte additive [29–33], high Li salt concentration [34], artificial protective layer for Li metal [35–38], high transference number electrolytes [39], nanoparticle hybrid electrolyte [40–42], all-carbon anode [43], structured metal anode [44,45], carbon [43,46–48]/silicon [49,50] based metal anode, hybrid anode structure [51,52], gel/solid electrolyte [53–55], and nanostructured framework [27,56,57] have been proposed.

The above-mentioned concepts effectively render a Li-S coin cell to more than 500 cycles with a discharging capacity of  $600\text{--}800 \text{ mAh g}^{-1}$  and a Coulombic efficiency of  $92\text{--}99\%$ . However, most of tests were achieved with a sulfur loading below  $70\%$  and an areal density below  $2.0 \text{ mg cm}^{-2}$  [58,59]. When the sulfur content in the cathode side is increased to  $4.0\text{--}10.0 \text{ mg cm}^{-2}$  for practical cells with high energy density, a large number of LiPS generates, dissolves into the electrolyte, and diffuses to the anode in a working cell [60]. A dramatic increase of LiPS concentration in the electrolyte induces rapid capacity decay and a low Coulombic efficiency even under the protective role of  $\text{LiNO}_3$  additive. The lifespan of the cell is severely limited. When the failed cell is disassembled, the shine Li metal anode becomes dark and the cell is almost dry in most cases. Attributed from the dynamic behavior of LiPSs in the electrolyte and complexity of a working cell based on conversion chemistry of Li and S active materials, the actual degradation mechanism, especially the failure of Li metal anode is a grand challenge.

Relative to the conventional Li metal-based batteries based on intercalation chemistry in conventional metal oxide cathode, dendrite issues in Li-S batteries are more serious and complicated due to the multi-electron conversion chemistry based on LiPS [61].

On one hand, the dissolved and shuttled LiPSs react with Li metal chemically to form  $\text{Li}_2\text{S}_2$  and  $\text{Li}_2\text{S}$  in the anode side. The low reactivity of  $\text{Li}_2\text{S}_2$  and  $\text{Li}_2\text{S}$  break away from the conductive matrix, resulting in irreversible capacity loss. On the other hand, the shuttled LiPSs participate in the formation of solid electrolyte interphase (SEI) [62–64], which is critically important for even Li depositing and therefore to improve the cycling efficiency. Consequently, LiPS intermediates are regarded as a double-edged sword in Li-S batteries. Exploring the positive role of LiPSs on the Li metal anode is not only critically important to suppress dendrite growth in anode side, but also fundamentally important to understand the shuttle behavior of a working Li-S battery, and thus to improve the discharging capacity, Coulombic efficiency, and long-term stability of practical Li-S cells.

In this contribution, we systematically investigated the role of LiPSs on the Li metal anode in a working Li-S battery. There are always continuous composition and concentration fluctuation of LiPSs in a working Li-S cell during charge/discharge cycle (Fig. 1a). Therefore, the role of polysulfides on the Li metal anode is very difficult to be clearly identified in a real Li-S cell. To mimic the actual composition of working cells and simplify the Li-S system,  $\text{Li}_2\text{S}_5$  was selected as model LiPS in a Li-Cu half-cell to probe the role of LiPS on Li metal anode (Fig. 1b). Herein,  $\text{Li}_2\text{S}_5$  with different concentrations was synthesized in the mostly accepted electrolyte (LiTFSI (1.0 M)-5.0 wt %  $\text{LiNO}_3$ -DOL/DME (1:1, in volume)) for practical Li-S batteries. A high  $\text{Li}_2\text{S}_5$  concentration electrolyte corresponds to a Li-S cell with high areal loading of sulfur in the cathode. The electrochemical performance based on electrolyte

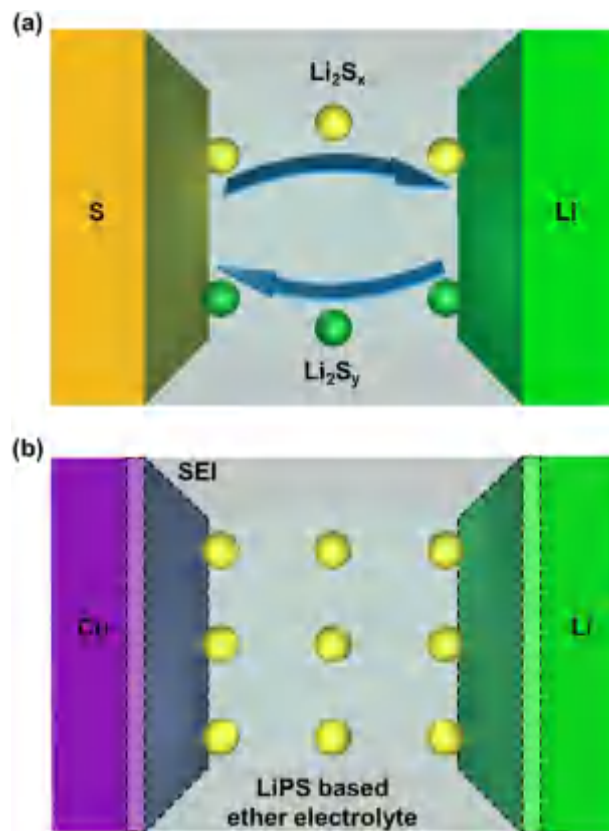


Fig. 1. Proof-of-concept of the role of LiPS on Li metal anode in a Li-S cell: (a) Conventional Li-S full cell, (b) designed Li|Cu half-cell with LiPS electrolyte to clearly discuss the role of LiPS on Li metal anode.

with different concentrations of LiPSs, such as aggressive-charging test and the related Li deposit morphology, long-term cycling test, and surface chemistry analysis, were comprehensively explored in a half cell with Li metal electrode. We found that the electrolyte with a sulfur concentration of 0.10 M rendered an unprecedented dendrite-free morphology, extraordinary Coulombic efficiency, and superior long-term stability. When the sulfur concentration in the electrolyte was improved to 1.0 M, the cell showed a severe decay in Coulombic efficiency and span life. A failure mechanism of high loading Li-S batteries and a strategy to protect the Li metal anode was proposed based on the interaction of LiPS with Li metal anode.

## 2. Experimental section

### 2.1. Preparation of LiPS electrolytes

The routine ether electrolyte was composed of 1.0 M LiTFSI in a mixed solvent of DME and DOL ( $v/v = 1:1$ ) (from Beijing Chemical Industry Group CO., LTD, with water content lower than 20 ppm) with 5.0 wt % of lithium nitrate ( $\text{LiNO}_3$ ) (from Alfa Aesar). The polysulfide-based electrolytes with different sulfur concentrations were fabricated by adding certain amount of  $\text{Li}_2\text{S}_5$  solution to the electrolyte. The  $\text{Li}_2\text{S}_5$  solution was prepared with the stoichiometric addition of  $\text{Li}_2\text{S}$  (from Alfa Aesar) and element sulfur.

### 2.2. Electrochemical measurements

The Li | electrolyte | Cu cells were employed to investigate the plating/stripping process which assembled in the 2025-type coin cells (MTI Corporation), composing of Li metal electrode and Cu foil electrode as substrate. Besides, STC24 dismountable cells (MTI Corporation) were specially customized to obtain the short circuit time while with the circinate Teflon separator (0.2 mm in thickness) in a battery. All cells were assembled in an Ar-filled glove box with  $\text{O}_2$  and  $\text{H}_2\text{O}$  content below 5.0 ppm. The 2025-type coins were tested in a galvanostatic mode at a current density of  $1.0 \text{ mA cm}^{-2}$  within a voltage range of  $-0.5 \text{ e } 0.5 \text{ V}$  with Neware multichannel battery cycler. The aggressive test to record short circuit time by using STC24 dismountable cells is at a current density of  $0.50 \text{ mA cm}^{-2}$ . The electrolyte conductivity and interfacial resistance is tested via EIS measurement ( $0.1 \sim 10^5 \text{ Hz}$ ) with Solartron 1470E electrochemical workstation. The diffusion resistance of Li ions through the SEI layer ( $R_{\text{SEI}}$ ) is obtained from an equivalent circuit fitted for the impedance spectra as our previous publication [61].

### 2.3. Characterization

The morphology of Li deposition/dissolution was characterized by a JSM 7401F SEM operated at 3.0 kV. We use Al- $K_{\alpha}$  radiation (72 W, 12 kV) at a pressure of  $10^{-9}$  torr and an argon ion beam (accelerating voltage 2.0 kV, ion beam current 6.0 mA, leading to an etching rate between 5 and  $50 \text{ \AA min}^{-1}$ ). All of the XPS spectra were calibrated by the carbon contamination using C1s peak (284.6 eV). The XPS spectra were analyzed using a nonlinear Shirley-type background. The X-ray spectra were obtained after 100 s etching process to be more accurate to characterize the SEI and avoid the effect of surface contamination. The diameter of the analyzed area was 400  $\mu\text{m}$ . The sample (Li deposits on Cu foil in the Li stripping state) was prepared in a glove box with a home-made container to avoid oxidation and parasitical reactions and they were transferred to the test machines.

## 3. Results and discussion

### 3.1. The short circuit test of Li metal anode in LiPS based electrolyte

In a routine coin cell, the growth behavior of Li dendrites is strongly affected by the polymer membrane closely attached with the Li anode. To eliminate the influence of the membrane and probe the intrinsic Li depositing behavior, a special cell configuration with a circinate Teflon separator [61] was employed in this work. The electrochemical performance of Li anode in LiPS based electrolyte was systematically investigated in a two-electrode cell with detachable configuration. The Li deposits grow in the ring-shaped aperture until reaching the cathode side without any barriers. Consequently, the overcharging performance of LiPS electrolyte by continuous Li depositing onto the anode current collector is experimentally recorded.

$\text{Li}_2\text{S}_5$  with sulfur concentrations of 0.0050, 0.010, 0.050, 0.10, 0.20, 0.50, and 1.0 M in LiTFSI (1.0 M)-5.0 wt%  $\text{LiNO}_3$ -DOL/DME were employed as model electrolytes. Such LiPS based electrolyte was synthesized from the stoichiometric reaction of  $\text{Li}_2\text{S}$  and  $\text{S}_8$  in ether-based electrolyte. The as-obtained LiPS based electrolyte exhibited an increased darkness in color with increasing sulfur concentration (Fig. S1).

Generally, both Li dendrite growth and final short circuit induce a sharp decrease in cell voltage during Li depositing. We recorded the profile of voltage vs Li depositing duration at  $0.50 \text{ mA cm}^{-2}$  to achieve the short circuit time. As shown in Fig. 2, the voltage curve indicated an obvious decrease after short circuit. Two kinds of short circuit are exhibited in the voltage curve: local and cell short circuit. The local short circuit is ascribed to the fact that a short circuit happens locally but the cell can work well. This is because Li dendrites just grow with a small amount and do not fill the cell completely. When Li dendrites break away from the counter electrode due to some reasons including stress-induced collapse of Li dendrites, the cell can be healed from local short circuit and work well again. However, when cell short circuit happens, dendrites completely fill the cell and damage the cell irreversibly. The local short circuit here is to indicate the time for Li dendrite nucleation, while the cell short circuit is to describe the final state of cells induced by the growth of a large quantity of Li dendrites. The short circuit times vary considerably with the concentration of LiPS. With sulfur concentrations of 0.0050, 0.010, 0.050, 0.10, 0.20, 0.50, and 1.0 M, the cells are with local short circuit times of 0.5, 2.6, 1.9, 2.7, 1.7, 1.7, and 1.7 h as well as cell short circuit times of 2.2, 2.7, 1.9, 4.5, 4.1, 4.0, and 5.1 h, respectively. Clearly, the cell with a sulfur concentration of 0.10 M affords the best performance in suppressing dendrite growth based on the local and cell short circuit time. When the sulfur concentration is increased to 0.20, 0.50, and 1.0 M, Li dendrites form on the anode, clearly demonstrated by the local short circuit time. The relatively high cell short circuit time for the high sulfur concentration electrolyte is attributed to the chemical reactions between Li dendrites and LiPSs. These reactions can decrease the length of Li dendrite and render Li dendrites out of contact with counter electrode, leading to the recovery of cell from short circuit. Though these reactions can relieve the dendrite-induced short circuit, a large amount of dead Li particles generate. The resulted dead Li not only decrease the active materials of Li metal in the anode and LiPS in the cathode, but also increase the Li ion diffusion resistance, thus badly deteriorating the cycling performance.

### 3.2. The surface morphology of Li metal after continuous Li depositing

The continuous Li depositing morphology after 3.0 h is shown as

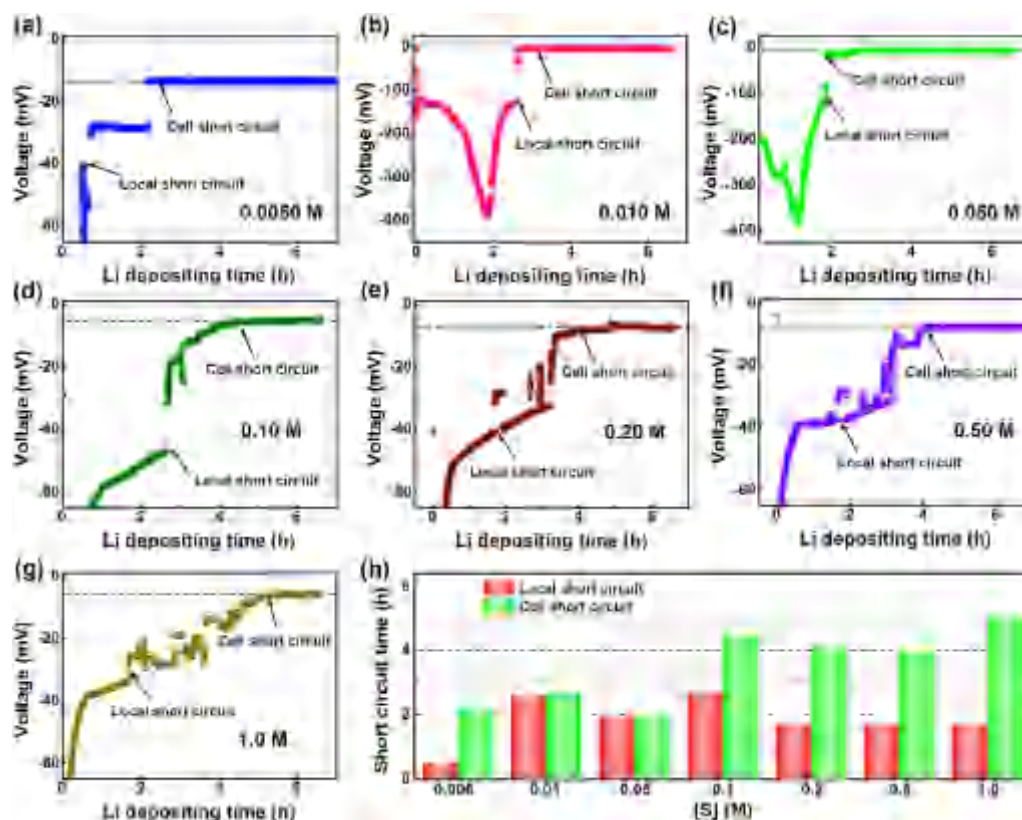


Fig. 2. The short circuit test for Li/Cu cells with polysulfide-based electrolytes. The voltage curves at  $0.50 \text{ mA cm}^{-2}$  are recorded during continuous Li depositing in the LiPS based electrolyte with [S] of (a) 0.0050 M, (b) 0.010 M, (c) 0.050 M, (d) 0.10 M, (e) 0.20 M, (f) 0.50 M, (g) 1.0 M. (h) The dependence of short circuit duration on sulfur concentration.

Fig. 3. Although no large dendrite is observed in LiPS based electrolyte with a sulfur concentration of 0.01 M, there are many tiny dendrite seeds of Li deposits with a size of ca.  $1.0 \text{ }\mu\text{m}$ . The dendrite seeds huddle together into the suborbicular structure. The seeds are nucleation sites for the following reduction of Li ions and therefore result in continuous growth of Li dendrites. For the Li anode working in a LiPS based electrolyte with a sulfur concentration of 0.10 M, the surface of the Li metal after Li deposition for 3.0 h at  $0.50 \text{ mA cm}^{-2}$  is relatively smooth. No large dendrite seed is found (Fig. 3c). This extends the short circuit time and is thus promising in enhancing the safety of the Li metal battery. However, when the sulfur concentration is further increased to 0.50 M, many large Li dendrites grow on the surface of Li metal. Li dendrites of  $1.5 \text{ }\mu\text{m}$  in diameter and tens of microns in length result in a quick local short circuit at a depositing duration of 1.7 h.

The aggressive-charging test clearly indicates that the Li metal deposition is strongly depended on the concentration of LiPSs in a working Li-S cell. A 0.10 M [S] electrolyte effectively suppresses Li dendrite growth. When the concentration of LiPS rises, a plenty of large Li dendrites grows on the Li metal anode. This is corresponding to a Li-S cell with a high areal sulfur loading in the cathode, in which the in-situ formed highly concentrated LiPS shuttles to the anode and induces the formation of Li dendrite and related poor safety issue.

### 3.3. The electrochemical cycling of Li metal in LiPS electrolyte

The Coulombic efficiency of a Li metal battery with LiPS based electrolyte was further investigated by the electrochemical behavior of Li plating/stripping and the cycling stability under the galvanostatic discharge/charge mode in Cu-Li coin cells (Fig. 4).

The Coulombic efficiency during Li plating/stripping in LiPS based electrolyte with different sulfur concentrations was shown in Fig. 4a. The Coulombic efficiency herein is defined by the ratio of the amount of lithium stripped (calculated based on charging capacity) and the amount of lithium plated (calculated based on the discharging capacity) on the stainless steel foil in a coin cell with Cu foil current collector as the cathode and the Li foil as the anode. The cell with 0.10 M [S] LiPS based electrolyte represents the best long-term cycling stability with a very high Coulombic efficiency of 97%. When the [S] is higher or lower than 0.10 M, both cycling stability and the Coulombic efficiency progressively degrades as the concentration deviates away from 0.10 M.

We define the duration at which the Coulombic efficiency is below 95% as the end of the cell service life. Fig. 4b exhibits the cell service life of LiPS electrolyte at different sulfur concentrations. The cells with sulfur concentrations of 0.0050, 0.010, 0.050, 0.10, 0.20, 0.50, and 1.0 M are respectively with lifespans of 93, 81, 143, 233, 200, 31, and 42 cycles at a current of  $1.0 \text{ mA cm}^{-2}$  and a capacity of  $1.0 \text{ mAh cm}^{-2}$ . The poor lifespan of high sulfur concentration electrolytes confirms the destructive role of high sulfur loading on the Li metal anode, thus deteriorating the cell performance. The polysulfide concentration in the electrolyte is critically important in forming a highly stable SEI, and thus the superior cycling performance of Li metal anode.

The formation of a stable SEI is also reflected by cell polarization and its dynamical evolution with cycling test. The initial charging-discharging curves are discussed for LiPS based electrolyte measured at  $1.0 \text{ mA cm}^{-2}$  (Fig. 4c). The polarization and initial Coulombic efficiency of these cells at this stage of cycling are nearly identical with  $70 \pm 80 \text{ mV}$  and  $75 \pm 85\%$ , respectively. A relatively stable SEI layer can form in the initial cycle for Li anode in every

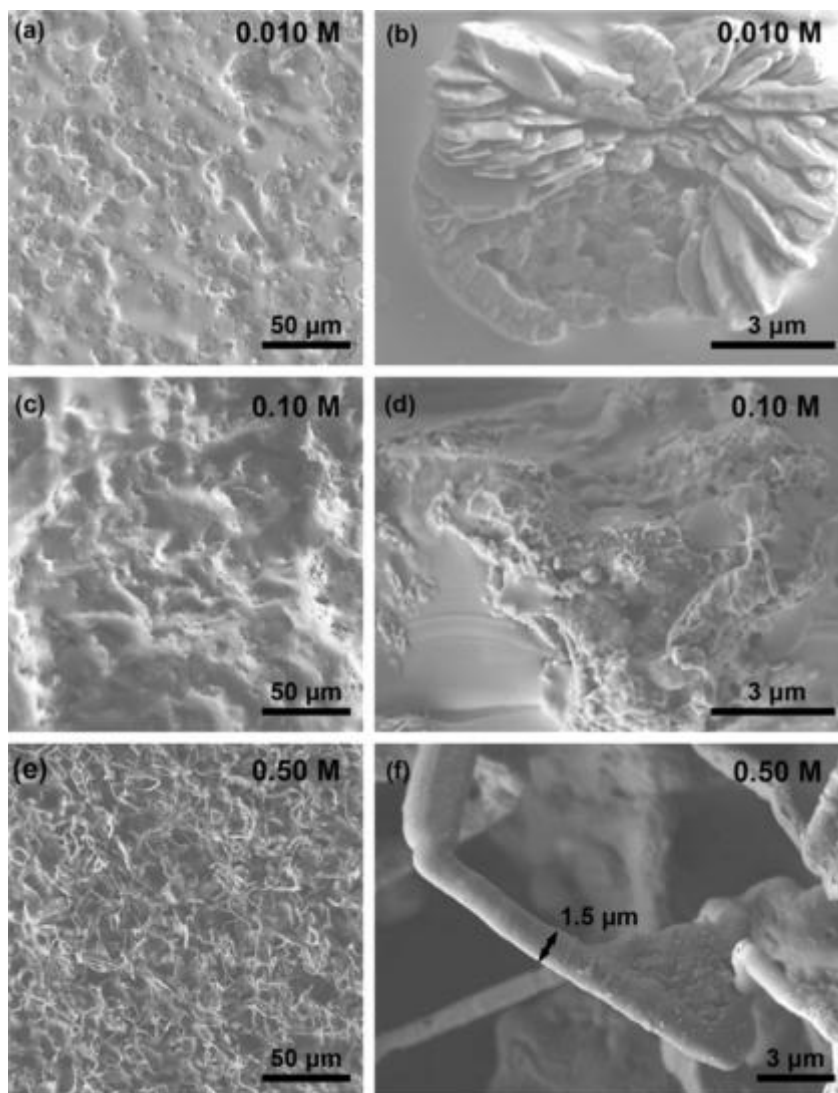


Fig. 3. The morphologies of Li surface after 3.0 h Li depositing at  $0.5 \text{ mA cm}^{-2}$  in the short circuit test. The SEM images of Li deposits with sulfur concentrations of (a, b) 0.010 M, (c, d) 0.10 M, and (e, f) 0.50 M. (b), (d), and (f) are the representative morphologies of regional enlarged views in (a), (c), and (e).

LiPS based electrolyte, which can be confirmed by the superior cycling performance in the initial 35 cycles (Fig. 4a). However, the long-term SEI stability is highly depended on the [S] concentration in LiPS based electrolyte. The poor SEI stability gives rise to the high parasitic reactions between electrolyte and Li metal, and result in very low Coulombic efficiency of the cell.

To investigate the synergy between  $\text{LiNO}_3$  and LiPS in the electrolyte on the Li metal anode, a control test with  $\text{LiNO}_3$  alone as the electrolyte additive without LiPS was conducted. The cells exhibit a stable and high Coulombic efficiency with the rise of  $\text{LiNO}_3$  concentration from 0, 0.10, 0.50, 1.0, 2.0, to 5.0 wt % (Fig. S2a). The electrolyte with a very high  $\text{LiNO}_3$  concentration of 5.0 wt % cannot maintain a high Coulombic efficiency after 120 cycles, which is consisted with published reports [64]. In contrast, a 0.020 M  $\text{Li}_2\text{S}_5$  (0.10 M sulfur)-5.0 wt %  $\text{LiNO}_3$  based electrolyte maintains a Coulombic efficiency of 95% even after 233 cycles. Consequently, the superior long-term cycling stability in Fig. 4a with 0.020 M  $\text{Li}_2\text{S}_5$  (0.10 M sulfur)-5.0 wt %  $\text{LiNO}_3$  is not induced by 5.0 wt %  $\text{LiNO}_3$  alone.

We also fixed the sulfur concentration at 0.10 M and changed the  $\text{LiNO}_3$  concentration from 0, 0.10, 0.50, 1.0, 2.0, to 5.0 wt %. The

0.020 M  $\text{Li}_2\text{S}_5$  (0.10 M sulfur)-5.0 wt %  $\text{LiNO}_3$  electrolyte demonstrates the best performance, while the other electrolytes cannot render the cells with more than 140 cycles (Fig. S2b). These control tests unambiguously confirm the effective and synergetic role of 0.020 M  $\text{Li}_2\text{S}_5$  (0.10 M sulfur)-5.0 wt %  $\text{LiNO}_3$  in building a very stable SEI layer to improve the Coulombic efficiency and life span.

The Li depositing and stripping morphology after 60 cycles were tracked by SEM images. When the Li metal was applied in a routine cell with polymer separator, the Li deposits are mechanically flattened (Fig. S3). However, the Li deposits in a cell with 0.10 M sulfur content is very dense, while the Li deposits in the cells with 0.010 and 0.50 M sulfur become loose. The dense Li deposits are beneficial for improving the volume energy density and reducing the amounts of dead Li, therefore improving the Coulombic efficiency. After Li stripping, Li metal loses electrons and is oxidized into Li ions. The Li ions vanish from the current collector, leaving a SEI layer on the surface of Li metal. The SEI layer formed in the 0.10 M sulfur electrolyte efficiently covers current collector. However, there are many wrinkles on the SEI layer formed in the 0.010 and 0.50 M electrolyte, which may be induced by the stress in the junctions of loose Li deposits. The wrinkles induce the unstable

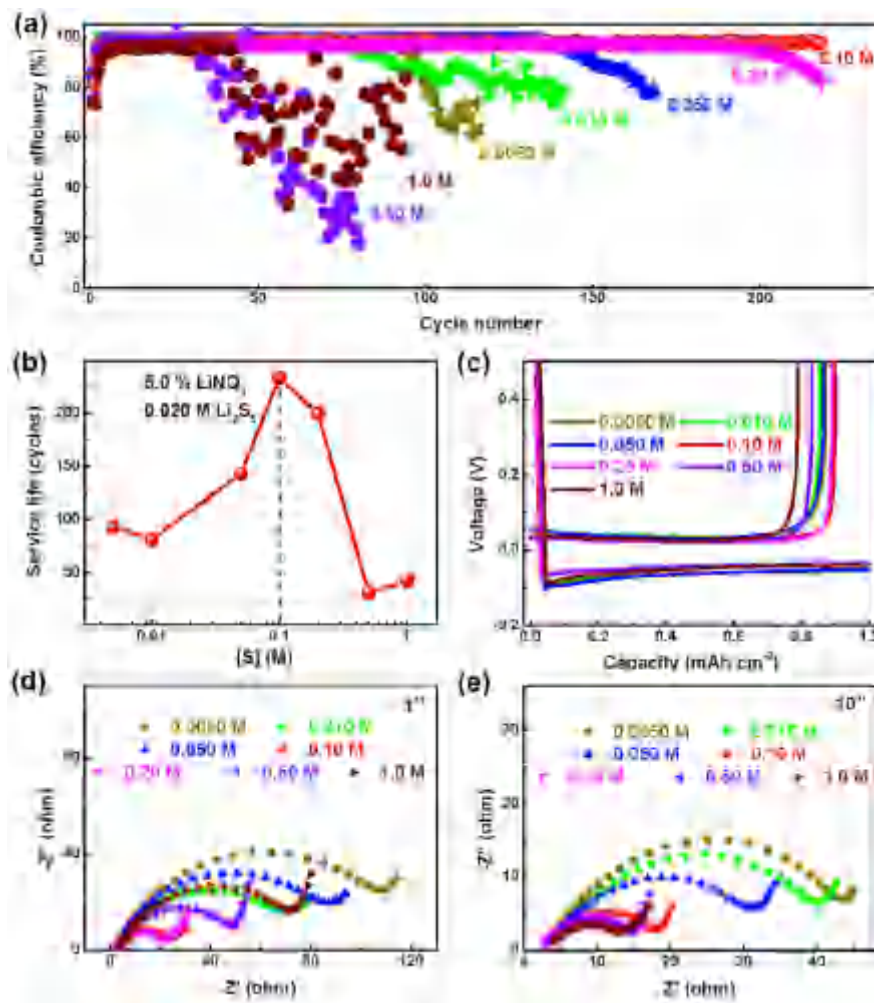


Fig. 4. Cycling performance of Li/Cu cells with LiPS-based electrolytes. (a) Coulombic efficiencies of Li/Cu cells at a current density of  $1.0 \text{ mA cm}^{-2}$  and a capacity of  $1.0 \text{ mAh cm}^{-2}$ . (b) The dependence of lifespan of Li/Cu cells in electrolytes upon the concentrations of  $\text{Li}_2\text{S}_5$ . (c) The 1st charging/discharging curves during Li depositing/stripping of Li/Cu cells. EIS of Li/Cu cells after (d) 1st and (e) 10th Li stripping.

cycling performance of the cell during the following cycling.

The electrical impedance spectrum (EIS) was employed to probe the diffusion resistance of Li ions through the SEI layer ( $R_{\text{SEI}}$ ) formed in LiPS based electrolyte after 1st and 10th cycle (Fig. 4d&e). The cell in 0.10 M sulfur electrolyte exhibits a  $R_{\text{SEI}}$  of 20  $\Omega$ , which is similar to that of 0.20 M sulfur electrolyte. However, cells with other LiPS based electrolytes display a very large  $R_{\text{SEI}}$  of 50–120  $\Omega$ . After 10 cycles,  $R_{\text{SEI}}$  of every cell with LiPS based electrolyte with different sulfur concentrations decreases due to the self-optimization of SEI layer during cycling. The  $R_{\text{SEI}}$  of the cell with 0.10 M sulfur electrolyte changes little, indicating the as-obtained SEI layer on the Li metal anode is well preserved (Fig. 4a). However, cells with other sulfur concentrations are with large variations in  $R_{\text{SEI}}$ , especially for high [S] electrolyte. The labile diffusion resistance also confirms the unstable SEI layer formed in high [S] electrolyte, which is directly responsible for the poor long-term cycling performance (Fig. 4b).

Based on Coulombic efficiency and long-term stability of Li metal anode in Cu-Li coin cells, 0.10 M [S] LiPS based electrolyte is with the best cycling performance. Both 0.005 and 1.0 M electrolyte leads to very low efficiency and short service life. Meanwhile, when the areal sulfur loading is too high in a Li-S battery, high concentration LiPSs will generate, which will inevitably shuttle to the

anode surface. Such highly concentrated LiPS can corrode the Li metal anode and lead to low utilization of sulfur and poor lifespan of Li-S batteries.

#### 3.4. The surface chemistry of Li metal in LiPS electrolyte

To gain the new insights into cycling stability of Li metal anode in LiPS based electrolyte with different sulfur concentrations, the composition of the SEI was further probed by X-ray photoelectron spectroscopy (XPS) analysis. Fig. S4 manifests the XPS spectra of S 2p, O 1s, N 1s, Li 1s, C 1s, and F 1s collected on the Li metal electrode after 10th electrochemical cycles in the LiPS based electrolyte with sulfur concentrations of 0.010, 0.10, and 0.50 M. All the Li metal anodes in every LiPS based electrolyte exhibit nearly the same peak in spite of some difference in peak intensity. The Li metal anode in a LiPS and  $\text{LiNO}_3$  based electrolyte always have a SEI layer with  $\text{ROLi}$ ,  $\text{ROCO}_2\text{Li}$ ,  $\text{LiN}_x\text{O}_y$ ,  $\text{Li}_3\text{N}$ ,  $\text{Li}_2\text{S}_x$ ,  $\text{Li}_2\text{SO}_x$ , and  $\text{LiF}$  etc [61–64]. During initial cycles,  $\text{LiNO}_3$  oxides  $\text{Li}_2\text{S}_5$  to  $\text{Li}_2\text{SO}_x$ , and meanwhile is reduced to  $\text{LiN}_x\text{O}_y$ . The  $\text{Li}_2\text{S}$  is attributed to the spontaneous reaction between  $\text{Li}_2\text{S}_5$  and Li metal.  $\text{LiF}$  is attributed to the decomposition of LiTFSI salt.

Though with nearly the same species, yet the percentage for each species differ considerably for the SEI layer formed in

electrolytes with various sulfur concentrations (Fig. 5a&b). With increasing sulfur concentration, the percentage of S 2p in the SEI layer rises from 2.87 to 4.13%. This is attributed from the fact that high sulfur concentration in the electrolyte results in a high proportion of sulfur species in the SEI. However, when the [S] increased from 0.010 to 0.50 M, such 50-time increase in sulfur concentration in the electrolyte just render a 1.44-time increase in S 2p content in SEI layer. The phenomenon is very similar with N species. The percentage of N 1s in the SEI layer increases from 1.14 to 1.45% with the sulfur concentration rose from 0.01 to 0.50 M. The high sulfur concentration also renders large quantities of reduction for  $\text{LiNO}_3$ . 0.10 M sulfur in the electrolyte renders the lowest O 1s content in the SEI layer. As oxygen element mostly appears in organic species, the decrease in O 1s content indicates the increasing proportion of inorganic species in the SEI layer, which enhances the Li ion conductivity.

More importantly, a sharp and strong LiF peak (685.2 eV) in F 1s XPS spectra of the SEI layer strongly affirms the fact that Li polysulfides in the 0.10 M [S] electrolyte leads to the highest F content in

the SEI layer (Fig. S4c). LiF is a very important electrolyte additive to protect Li metal anode [65,66]. A LiF-rich SEI was obtained through in-situ reaction on Li metal anode in 0.10 M [S] electrolyte. The in-situ formed LiF content in the SEI layer significantly favors the long-term stability of Li depositing and stripping in a polysulfide containing ether electrolyte that is widely accepted for Li-S batteries.

### 3.5. The role of LiPS on Li metal in LiPS electrolyte

The multi-electron conversion chemistry between Li and S affords the Li-S cells with very high theoretical high capacity and energy density. However, the soluble polysulfide intermediates diffuse through the separator and react with fresh Li metal in an ether-based electrolyte. If a very stable SEI can be built on the interfaces between Li metal and electrolyte, the LiPSs can't attack fresh Li metal and continuously corrode the Li metal anode.

Herein, the Li metal anode in the electrolyte with 0.020 M  $\text{Li}_2\text{S}_5$  (0.10 M sulfur)-5.0 wt %  $\text{LiNO}_3$  demonstrates a dendrite-free morphology, superb Coulombic efficiency, and superior long-term

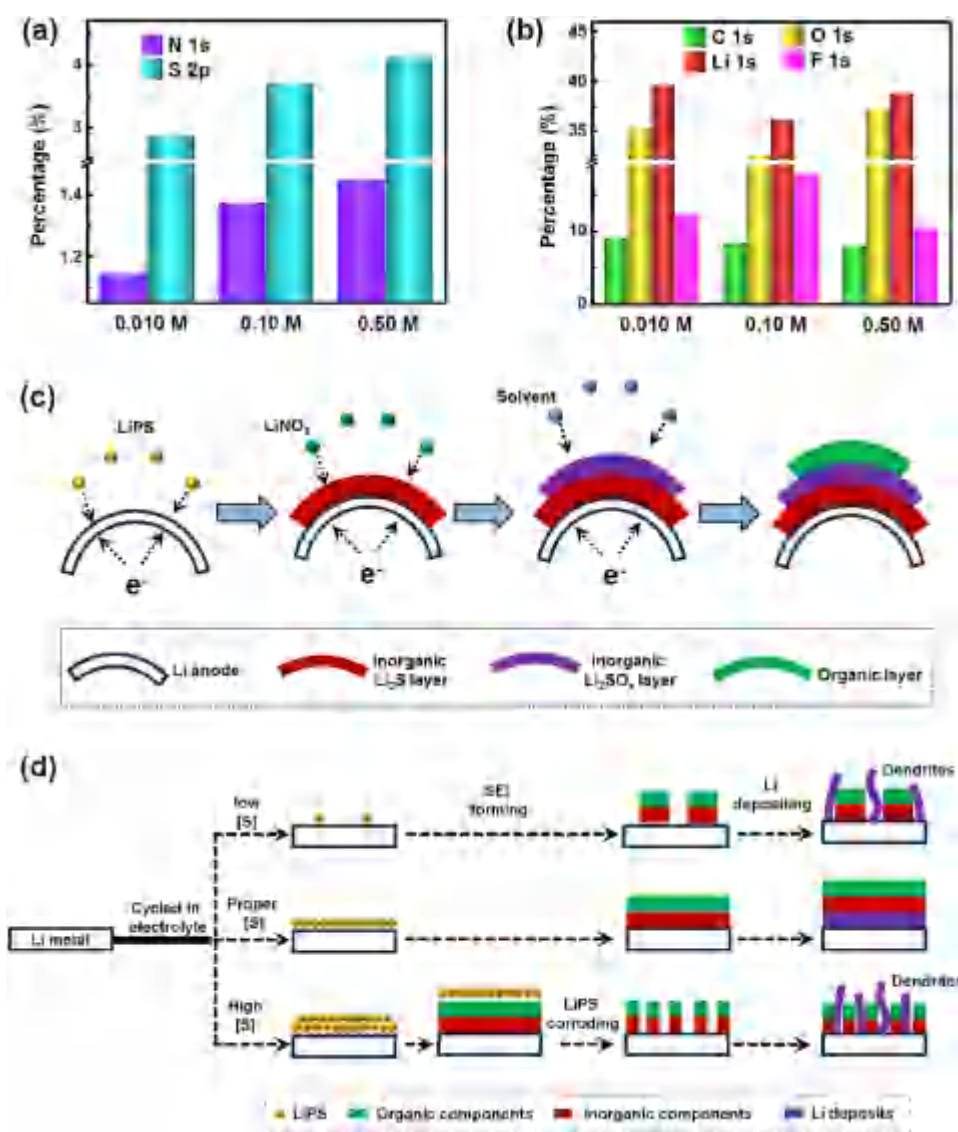


Fig. 5. The surface chemistry of Li metal anode and possible mechanisms of reaction in LiPS electrolyte. Element percentage of SEI layer formed in LiPS-based electrolytes with different [S] after 10th cycle: (a) S 2p & N 1s, (b) C 1s, O 1s, Li 1s and F 1s. Schematic illustrations describing (c) the possible mechanisms of SEI formation process in LiPS based electrolyte, and (d) the role of LiPS concentrations on SEI evolutions and Li depositing.

stability. When the fresh Li metal is exposed to the LiPS containing electrolyte, the rapid disproportionation reaction between  $\text{Li}_2\text{S}_5$  and Li induces a  $\text{Li}_2\text{S}$  layer at the interface of Li metal and organic electrolyte. With the addition of  $\text{LiNO}_3$  in the electrolyte, the  $\text{Li}_2\text{S}_5$  reduces  $\text{LiNO}_3$  into less oxidative  $\text{LiNO}_2$  upon initial formation of SEI. Therefore, a very complex SEI layer including of  $\text{LiN}_x\text{O}_y$ ,  $\text{Li}_3\text{N}$ ,  $\text{Li}_2\text{S}_x$ ,  $\text{Li}_2\text{SO}_x$ , and LiF is achieved in the  $\text{Li}_2\text{S}_5$ - $\text{LiNO}_3$  electrolyte. Organic components also formed due to decomposition of solvent (Fig. 5c). The as-obtained results are also confirmed by the XPS, transmission electron microscopy, and Auger electron spectroscopy reported in our previous work [62] and Xiong's results [63]. There are organic layer contacted with organic electrolyte and inorganic layer attached with Li metal in SEI. The organic layers were mainly derived from the decomposition of ether electrolyte into ROLi and  $\text{ROCO}_2\text{Li}$ , while the inorganic one with  $\text{LiN}_x\text{O}_y$ ,  $\text{Li}_3\text{N}$ ,  $\text{Li}_2\text{S}_x$ ,  $\text{Li}_2\text{SO}_x$ , and LiF is mainly originated from the complex reactions between the Li metal and salts in the electrolyte. The distribution of SEI is highly depended on the LiPS concentration in the LiPS electrolyte.

The soluble LiPSs will directly interact with Li metal anode. When the LiPS is in very low concentration ( $[\text{S}] < 0.050 \text{ M}$ ), the formation of a uniform SEI layer can hardly occur (Fig. 5d). As  $\text{Li}_2\text{S}$  prefers to form on the Li (110) plane first rather than Li (111) [67], the ultralow sulfur concentration cannot build a continuous SEI layer on Li metal. The mutable and cracked SEI layer exposes fresh Li metal surface as dendrite formation site on the anode. The SEI prefers to be stable at a very high amount of electrolyte and a relatively low LiPS concentration (0.10 M). When the sulfur concentration is very high ( $[\text{S}] > 0.50 \text{ M}$ ) in the ether electrolyte, the cell exhibits a severe decay in efficiency even under the protecting of 5.0 wt %  $\text{LiNO}_3$ . A large amount of shuttled LiPS severely corrodes Li metal, leading to the cracked SEI layer and severe dendrite growth. The Li metal is etched into black powders and the electrolyte is gradually consumed. The Li dendrites induce dead Li in anode side and trigger large diffusion resistance for Li ions and low efficiency of sulfur cathode, thus severe capacity decay and low Coulombic efficiency is observed for Li-S cell with high sulfur loading. These facts explain the reason why Li-S batteries with a very high areal sulfur loading often exhibit a very poor cycling life, even though  $\text{LiNO}_3$  is applied as anode protector. Consequently, cathode and membrane medications must be applied to decrease the sulfur content in the electrolyte in anode side to nearly 0.10 M in the electrolyte.

It should be noticed that results of Cu-Li half-cell with low sulfur concentration (0.0050 and 0.010 M) at 1.0  $\text{mAh cm}^{-2}$  exhibit a low Coulombic efficiencies after 100 cycles. In contrast, a working Li-S battery with ultralow sulfur loading ( $< 1.0 \text{ mg cm}^{-2}$ ) is commonly with a long cycle life around 300 cycles. It should be noticed that a low sulfur loading cell has a very low capacity ( $< 0.3 \text{ mAh cm}^{-2}$ ). An  $> 2000\%$  excessive Li anode relative to sulfur in the cathode is applied in 2025 or 2032 type coin cells [43]. Therefore, the Li metal in a Li-S battery with low sulfur areal loading is not severally used for conversion reaction and always affords a high discharging capacity and superior cycling stability. This is one main reason for the widely use of low areal sulfur loading cell to probe the intrinsic potential of conductive materials for Li-S batteries in most scientific research.

We reported a uniform deposition of continuous SEI in an electrolyte with 0.020 M  $\text{Li}_2\text{S}_5$  (0.10 M sulfur)-5.0 wt %  $\text{LiNO}_3$ . The LiPS additive with proper concentration induces perfect match among complex reactions of SEI formation, which results in the LiF-rich inorganic SEI with stable morphology. The detailed formation mechanism is still not clear yet. Novel dynamic characterization is urgently required and under developing to clarify the surface chemistry of SEI formation on Li metal surface. We conclude herein that except for the reaction products between LiPS and  $\text{LiNO}_3$

( $\text{Li}_2\text{SO}_x$  and  $\text{LiN}_x\text{O}_y$ ) confirmed in other literature, SEI with large quantities of inorganic LiF and  $\text{Li}_2\text{S}_x$  content is very stable in a Li-S system. As reported by Archer and co-workers, LiF is an effective additive for Li metal protecting in ether-based electrolyte [65,68]. Herein, the in-situ formed LiF species render the efficient and stable Li plating and stripping.

The insights reported in this contribution not only promote the fundamental understanding of the interaction between LiPS and Li metal anode in a Li-S battery, but also the relationship between electrolyte modification and protective SEI layer. We conclude the novel understanding into the three outstanding characteristics:

(1) A new failure mechanism of Li metal etching at a high sulfur loading in a Li-S cell. The very high concentration LiPSs ( $> 0.50 \text{ M}$  [S]) in the ether-based electrolyte etch the SEI layer and Li anode easily, resulting in the huge consumption of organic electrolyte. This is also confirmed by direct observation of Li metal failure in a Li-S cell with a very high sulfur loading of  $18.1 \text{ mg cm}^{-2}$  by Manthiram and co-workers [69]. Therefore, the control of LiPS dissolution and diffusion is very efficient to protect the Li anode from a systematic view. When designing the practical Li-S full cell at a very high sulfur loading, the cathode, separator, and electrolyte should be rationally integrated to regulate the LiPS transportation and guarantee a stable SEI on Li metal anode. Otherwise, the electrolyte additive cannot improve the cycling performance of high loading Li-S full cells during whole life span, though it can effectively protect the Li metal anode in half cells, such as the strongly protective  $\text{LiNO}_3$  additive.

(2) Excellent electrolyte additives for Li metal anode. 0.020 M  $\text{Li}_2\text{S}_5$  (0.10 M sulfur)-5.0 wt %  $\text{LiNO}_3$  based ether electrolyte indicates a superior cycling stability for Li metal anode after 233 cycles. It is the best record for  $\text{LiNO}_3$  based electrolyte for Li-Cu coil cells. The  $\text{Li}_2\text{S}_5$ - $\text{LiNO}_3$  based ether electrolyte is with enormous potentiality to well protect the Li metal anode with robust LiF/ $\text{LiS}_x$  riched SEI in working Li-S batteries.

(3) New understanding towards electrolyte additive design used in Li-S batteries.  $\text{LiNO}_3$  is considered as one of the most effective additives to protect the anode of Li-S batteries. However, when the sulfur loading in the cathode side is too high and too much LiPSs dissolve into the electrolyte and diffuse to the anode, the cycling performance of Li metal anode be heavily ruined. Consequently, when designing the electrolyte additive, the performance of Li-Cu half-cell without LiPSs is not convictive enough. Comprehensive consideration of Li metal protection and LiPS shuttle is absolutely essential for Li-S full cells with ultralong lifespan.

#### 4. Conclusions

In conclusion, the LiPSs participate in the formation of inorganic layers in the SEIs on Li metal in a widely accepted ether-based electrolyte. Li metal anode is well protected by the stable inorganic layer formed in an ether-based electrolyte containing 0.020 M  $\text{Li}_2\text{S}_5$  (0.10 M sulfur) and 5.0 wt %  $\text{LiNO}_3$ . The metal anode with LiF- $\text{Li}_2\text{S}_x$  riched SEI renders a stable Coulombic efficiency of 95% after 233 cycles for a Li-Cu half-cell. A dendrite-free morphology of Li metal anode is observed under the harsh condition. When the LiPS is with a very high concentration LiPS of higher than 0.50 M sulfur in the organic electrolyte, the in-situ formed SEI is not well maintained and the Li metal is gradually etched, leading to the growth of Li dendrites and low efficiency of Li metal anode. Therefore, the polysulfide dissolution and diffusion should be delicately regulated by strong anchoring onto conductive framework and permselective separator/interlayer to render a practical Li-S cell with a very high areal sulfur loading. The prospective herein not only affords new understanding on the complex roles of LiPSs on the Li anode, but also sheds fresh concepts to achieve safe and efficient electrolyte

additive for Li metal protection in a working Li-S battery.

## Acknowledgements

This work was supported by the Natural Scientific Foundation of China (21306103, 21422604, and 21561130151), National Basic Research Program of China (2015CB932500), and the Ministry of Science and Technology of the People's Republic of China (2016YFA0202500). We thank helpful discussion from Rui Zhang, Hong-Jie Peng, Xiang Chen, and Xiao-Ru Chen. We thank Hao-Fan Wang for illustration preparation.

## Appendix A. Supplementary data

Supplementary data related to this article can be found at <http://dx.doi.org/10.1016/j.jpowsour.2016.07.056>.

## References

- M.R. Palacin, A. de Guibert, *Science* 351 (2016) 574.
- X. Ji, K.T. Lee, L.F. Nazar, *Nat. Mater* 8 (2009) 500e506.
- Y.X. Yin, S. Xin, Y.G. Guo, L.J. Wan, *Angew. Chem. Int. Ed.* 52 (2013) 13186e13200.
- A. Manthiram, S.H. Chung, C.X. Zu, *Adv. Mater* 27 (2015) 1980e2006.
- Z. Li, Y.M. Huang, L.X. Yuan, Z.X. Hao, Y.H. Huang, *Carbon* 92 (2015) 41e63.
- J. Liang, Z.-H. Sun, F. Li, H.-M. Cheng, *Energy Storage Mater* 2 (2016) 76e106.
- M. Hagen, D. Hanselmann, K. Ahlbrecht, R. Maca, D. Gerber, J. Tuebke, *Adv. Energy Mater* 5 (2015) 1401986.
- R. Cao, W. Xu, D. Lv, J. Xiao, J.-G. Zhang, *Adv. Energy Mater* 5 (2015) 1402273.
- A. Rosenman, E. Markevich, G. Salitra, D. Aurbach, A. Garsuch, F.F. Chesneau, *Adv. Energy Mater.* 5 (2015) 1500212.
- W. Li, Z. Liang, Z. Lu, H. Yao, Z.W. Seh, K. Yan, G. Zheng, Y. Cui, *Adv. Energy Mater.* 5 (2015) 1500211.
- H.-J. Peng, J.-Q. Huang, M.-Q. Zhao, Q. Zhang, X.-B. Cheng, X.-Y. Liu, W.-Z. Qian, F. Wei, *Adv. Funct. Mater.* 24 (2014) 2772e2781.
- S. Xin, L. Gu, N.-H. Zhao, Y.-X. Yin, L.-J. Zhou, Y.-G. Guo, L.-J. Wan, *J. Am. Chem. Soc.* 134 (2012) 18510e18513.
- F. Xu, Z.W. Tang, S.Q. Huang, L.Y. Chen, Y.R. Liang, W.C. Mai, H. Zhong, R.W. Fu, D.C. Wu, *Nat. Commun.* 6 (2015) 7221.
- M.-Q. Zhao, H.-J. Peng, G.-L. Tian, Q. Zhang, J.-Q. Huang, X.-B. Cheng, C. Tang, F. Wei, *Adv. Mater* 26 (2014) 7051e7058.
- Q. Pang, D. Kundu, M. Cuisinier, L.F. Nazar, *Nat. Commun.* 5 (2014) 4759.
- M. Liu, F. Ye, W. Li, H. Li, Y. Zhang, *Nano Res.* 9 (2016) 94e116.
- Q. Pang, X. Liang, C.Y. Kwok, L.F. Nazar, *J. Electrochem. Soc.* 162 (2015) A2567eA2576.
- G.M. Zhou, Y.B. Zhao, A. Manthiram, *Adv. Energy Mater* 5 (2015) 1402263.
- J.X. Song, M.L. Gordin, T. Xu, S.R. Chen, Z.X. Yu, H. Sohn, J. Lu, Y. Ren, Y.H. Duan, D.H. Wang, *Angew. Chem. Int. Ed.* 54 (2015) 4325e4329.
- G.M. Zhou, L. Li, D.W. Wang, X.Y. Shan, S.F. Pei, F. Li, H.M. Cheng, *Adv. Mater* 27 (2015) 641e647.
- J.-Q. Huang, Q. Zhang, F. Wei, *Energy Storage Mater* 1 (2015) 127e145.
- F. Wu, Y.S. Ye, R.J. Chen, J. Qian, T. Zhao, L. Li, W.H. Li, *Nano Lett.* 15 (2015) 7431e7439.
- H. Kim, F. Wu, J.T. Lee, N. Nitta, H.-T. Lin, M. Oschatz, W.I. Cho, S. Kaskel, O. Borodin, G. Yushin, *Adv. Energy Mater* 5 (2015) 1401792.
- F. Wu, Q. Zhu, R. Chen, N. Chen, Y. Chen, Y. Ye, J. Qian, L. Li, *J. Power Sources* 296 (2015) 10e17.
- X. Liang, C. Hart, Q. Pang, A. Garsuch, T. Weiss, L.F. Nazar, *Nat. Commun.* 6 (2015) 5682.
- Z. Ma, X. Huang, Q. Jiang, J. Huo, S. Wang, *Electrochim. Acta* 182 (2015) 884e890.
- X.-B. Cheng, H.-J. Peng, J.-Q. Huang, F. Wei, Q. Zhang, *Small* 10 (2014) 4257e4263.
- S.-H. Chung, P. Han, R. Singhal, V. Kalra, A. Manthiram, *Adv. Energy Mater* 5 (2015) 1500738.
- D. Aurbach, E. Pollak, R. Elazari, G. Salitra, C.S. Kelley, J. Affinito, *J. Electrochem. Soc.* 156 (2009) A694eA702.
- C.X. Zu, N. Azimi, Z.C. Zhang, A. Manthiram, *J. Mater. Chem. A* 3 (2015) 14864e14870.
- C.X. Zu, A. Manthiram, *J. Phys. Chem. Lett.* 5 (2014) 2522e2527.
- J. Guo, Z.Y. Wen, M.F. Wu, J. Jin, Y. Liu, *Electrochem. Commun.* 51 (2015) 59e63.
- F. Ding, W. Xu, G.L. Graff, J. Zhang, M.L. Sushko, X. Chen, Y. Shao, M.H. Engelhard, Z. Nie, J. Xiao, X. Liu, P.V. Sushko, J. Liu, J.-G. Zhang, *J. Am. Chem. Soc.* 135 (2013) 4450e4456.
- L. Suo, Y.-S. Hu, H. Li, M. Armand, L. Chen, *Nat. Commun.* 4 (2013) 1481.
- X.-B. Cheng, T.-Z. Hou, R. Zhang, H.-J. Peng, C.-Z. Zhao, J.-Q. Huang, Q. Zhang, *Adv. Mater* 28 (2016) 2888e2895.
- G. Ma, Z. Wen, M. Wu, C. Shen, Q. Wang, J. Jin, X. Wu, *Chem. Commun.* 50 (2014) 14209e14212.
- N.-W. Li, Y.-X. Yin, C.-P. Yang, Y.-G. Guo, *Adv. Mater* 28 (2016) 1853e1858.
- K. Yan, H.-W. Lee, T. Gao, G. Zheng, H. Yao, H. Wang, Z. Lu, Y. Zhou, Z. Liang, Z. Liu, S. Chu, Y. Cui, *Nano Lett.* 14 (2014) 6016e6022.
- Y. Lu, M. Tikekar, R. Mohanty, K. Hendrickson, L. Ma, L.A. Archer, *Adv. Energy Mater* 5 (2015) 1402073.
- Y.Y. Lu, K. Korf, Y. Kambe, Z.Y. Tu, L.A. Archer, *Angew. Chem. Int. Ed.* 53 (2014) 488e492.
- S. Choudhury, R. Mangal, A. Agrawal, L.A. Archer, *Nat. Commun.* 6 (2015) 10101.
- Z.Y. Tu, P. Nath, Y.Y. Lu, M.D. Tikekar, L.A. Archer, *Accounts. Chem. Res.* 48 (2015) 2947e2956.
- J. Bruckner, S. Thieme, F. Bottger-Hiller, I. Bauer, H.T. Grossmann, P. Strubel, H. Althues, S. Spange, S. Kaskel, *Adv. Funct. Mater* 24 (2014) 1284e1289.
- J. Heine, S. Krüger, C. Hartnig, U. Wietelmann, M. Winter, P. Bieker, *Adv. Energy Mater* 4 (2014) 1300815.
- M.-H. Ryou, Y.M. Lee, Y. Lee, M. Winter, P. Bieker, *Adv. Funct. Mater* 25 (2014) 834e841.
- Z. Liang, D. Lin, J. Zhao, Z. Lu, Y. Liu, C. Liu, Y. Lu, H. Wang, K. Yan, X. Tao, Y. Cui, *Proc. Natl. Acad. Sci.* 113 (2016) 2862e2867.
- R. Zhang, X.-B. Cheng, C.-Z. Zhao, H.-J. Peng, J.-L. Shi, J.-Q. Huang, J. Wang, F. Wei, Q. Zhang, *Adv. Mater* 28 (2016) 2155e2162.
- D. Lin, Y. Liu, Z. Liang, H.-W. Lee, J. Sun, H. Wang, K. Yan, J. Xie, Y. Cui, *Nat. Nanotechnol.* 11 (2016) 626e632.
- M. Hagen, E. Quiroga-Gonzalez, S. Dorfler, G. Fahrner, J. Tubke, M.J. Hoffmann, H. Althues, R. Speck, M. Krampfert, S. Kaskel, H. Foll, *J. Power Sources* 248 (2014) 1058e1066.
- S.K. Lee, S.M. Oh, E. Park, B. Scrosati, J. Hassoun, M.S. Park, Y.J. Kim, H. Kim, I. Belharouak, Y.K. Sun, *Nano Lett.* 15 (2015) 2863e2868.
- C. Huang, J. Xiao, Y. Shao, J. Zheng, W.D. Bennett, D. Lu, L.V. Saraf, M. Engelhard, L. Ji, J. Zhang, X. Li, G.L. Graff, J. Liu, *Nat. Commun.* 5 (2014) 3015.
- C.P. Yang, Y.X. Yin, S.F. Zhang, N.W. Li, Y.G. Guo, *Nat. Commun.* 6 (2015) 8058.
- Q.S. Wang, Z.Y. Wen, J. Jin, J. Guo, X. Huang, J.H. Yang, C.H. Chen, *Chem. Commun.* 52 (2016) 1637e1640.
- Z. Lin, C.D. Liang, *J. Mater. Chem. A* 3 (2015) 936e958.
- D. Zhou, R. Liu, Y.-B. He, F. Li, M. Liu, B. Li, Q.-H. Yang, Q. Cai, F. Kang, *Adv. Energy Mater* 6 (2016) 1502214.
- X. Zhang, W. Wang, A. Wang, Y. Huang, K. Yuan, Z. Yu, J. Qiu, Y. Yang, *J. Mater. Chem. A* 2 (2014) 11660e11665.
- G.Y. Zheng, S.W. Lee, Z. Liang, H.W. Lee, K. Yan, H.B. Yao, H.T. Wang, W.Y. Li, S. Chu, Y. Cui, *Nat. Nanotechnol.* 9 (2014) 618e623.
- X.-B. Cheng, J.-Q. Huang, H.-J. Peng, J.-Q. Nie, X.-Y. Liu, Q. Zhang, F. Wei, *J. Power Sources* 253 (2014) 263e268.
- D.W. Wang, Q.C. Zeng, G.M. Zhou, L.C. Yin, F. Li, H.M. Cheng, I.R. Gentle, G.Q.M. Lu, *J. Mater. Chem. A* 1 (2013) 9382e9394.
- D. Lv, J. Zheng, Q. Li, X. Xie, S. Ferrara, Z. Nie, L.B. Mehdi, N.D. Browning, J.-G. Zhang, G.L. Graff, J. Liu, J. Xiao, *Adv. Energy Mater* 5 (2015) 1402290.
- X.-B. Cheng, H.-J. Peng, J.-Q. Huang, R. Zhang, C.-Z. Zhao, Q. Zhang, *ACS Nano* 9 (2015) 6373e6382.
- C.-Z. Zhao, X.-B. Cheng, R. Zhang, H.-J. Peng, J.-Q. Huang, R. Ran, Z.-H. Huang, F. Wei, Q. Zhang, *Energy Storage Mater* 3 (2016) 77e84.
- S. Xiong, K. Xie, Y. Diao, X. Hong, *J. Power Sources* 246 (2014) 840e845.
- W. Li, H. Yao, K. Yan, G. Zheng, Z. Liang, Y.-M. Chiang, Y. Cui, *Nat. Commun.* 6 (2015) 7436.
- Y.Y. Lu, K. Korf, Y. Kambe, Z.Y. Tu, L.A. Archer, *Angew. Chem. Int. Ed.* 53 (2014) 488e492.
- R. Miao, J. Yang, X. Feng, H. Jia, J. Wang, Y. Nuli, *J. Power Sources* 271 (2014) 291e297.
- Z. Liu, S. Bertolini, P.B. Balbuena, P.P. Mukherjee, *ACS Appl. Mater. Interfaces* 8 (2016) 4700e4708.
- S. Choudhury, L.A. Archer, *Adv. Electron. Mater* 2 (2016) 1500246.
- L. Qie, C. Zu, A. Manthiram, *Adv. Energy Mater* 6 (2016) 1502459.